

On the derivation of coseismic displacement fields using
differential radar interferometry: the Landers earthquake

HOWARD A. ZEBKER, PAUL ROSEN, RICHARD M.
GOLDSTEIN, ANDREW GABRIEL, AND CHARLES L. WERNER

*Jet Propulsion Laboratory
California Institute of Technology
4800 Oak Grove Drive
Pasadena, CA 91109*

1 December 1, 1993

To be submitted to:
JGR Earth

Please address correspondence to:

Howard A. Zebker

MS 300-227

Jet Propulsion Laboratory

4800 Oak Grove Drive

Pasadena, CA 91109

Tel. (818) 354-8780, FAX (818) 393-5285

Abstract.

We develop here a map of the coseismic displacement field resulting from the Landers, CA, June 28, 1992 earthquake derived using data acquired from an orbiting high resolution radar system only, and achieve results more accurate than previous space studies and similar in accuracy to those obtained by conventional field survey techniques. Data from the ERS-1 synthetic aperture radar instrument acquired in April, July, and August 1992 are used to generate a high resolution wide area map of the displacements. The data represent the motion in the direction of the radar line of sight to cm level precision of each 30 m resolution element in a 100 km by 100 km image. Our coseismic displacement contour map gives a lobed pattern consistent with theoretical models of the displacement field from the earthquake. Fine structure observed as displacement tiling in regions several kilometers from the fault appears to be the result of local surface fracturing. Comparison of these data with GPS and EDM survey data show that either the two values agree within 10 cm on an absolute scale or within $\approx 30\%$ on a relative scale, thus the radar measurements are a means to extend the point measurements acquired by traditional techniques to an area map format. The technique we use is i) more automatic, ii) more precise, and iii) better validated than previous similar applications of differential radar interferometry. Since we require only remotely-sensed satellite data with no additional requirements for ancillary information, the technique is better suited for global seismic monitoring and analysis.

Introduction

Interferometric radar techniques for the generation of highly accurate digital elevation models (DEMs) have by now been well-documented in the literature (Zebker and Goldstein, 1986; Goldstein et al., 1988; Prati et al., 1990; Zebker et al., 1992; Evans et al., 1992; Madsen et al., 1993a; Madsen et al., 1993b; Zebker et al., 1993), as has been the application of such techniques to the measurement of the motion of all resolved points in a remotely-sensed image (Goldstein and Zebker, 1987; Goldstein et al., 1989). These related techniques follow from analysis and interpretation of interferograms, which consist of the phase differences between two radar images of the same scene acquired at separate locations or times - a sensor location change gives sensitivity to topography and a sensor temporal change gives motion sensitivity. A combination of the two approaches, denoted differential radar interferometry since the phase measurements of interest result from the difference of two interferograms, has previously been used by Gabriel et al. (1988) to map the changes in surface elevation of agricultural fields over a large area to cm-level sensitivities.

More recently, there has been activity by at least two groups applying the capabilities of radar interferometry to the study of seismic phenomena. Massonet et al. (1993) of Centre National d'Etudes Spatiales (CNES) in Toulouse, France used an interferometric digital elevation model derived from ERS-1 satellite data for analysis of the magnitude 7.3 earthquake centered near Landers, CA on June 28, 1992. In this study a single interferogram which contained phase signals from the local topography and from the earthquake displacements was subtracted from a manipulate USGS

15 minute DEM of the area and the residual phases interpreted as ground displacements from the event. The interferogram, when corrected for topographic effects, shows a displaced dual-lobed pattern of fringes emanating from the fault zone, where each fringe represents about 2.8 cm of motion in the radar line of sight direction. They also derive a theoretical fringe pattern from a model of the [earthquake motion which matches the observations fairly closely,

There are several important limitations in the above study. Although a USGS 90 m spacing 1 DEM was available for this site, for many sites in the world no DEM exists. In addition, an existing DEM may not be sufficiently accurate to yield the desired precision. The CNES team estimate a precision in their measurements of about 2.8 cm in the radar line of sight motion, limited mainly by imprecision in the USGS DEM plus radar system noise. Also, the DEM must be precisely coregistered to the radar image, which itself may be a difficult task (see Madsen et al., 1993b, for more on errors induced by DEM misregistration). Finally, since the interferogram phases are all measured modulo 2π , the absolute, or even relative, phase relationship between arbitrary points in the scene is difficult to determine. Thus, it is virtually impossible to fit continuous two-dimensional models of the displacement field to the observations.

These limitations aside, it is important to realize that the phase displacements due to motion in an interferometric DEM can be hundreds of times more sensitive than simply differencing the actual height measurements before and after an event (see below). This observation is what gives the interferometric approach the ability to map cm scale distortions over a region many tens of kilometers in size at a resolution of a few meters.

In this paper, we approach the Landers analysis differently from Massonet et al. by utilizing only data acquired by the ERS-1 satellite. Our motivations for doing this are both technical and philosophical. While reference DEM data are available for the Landers site, reliance on them in general for interferometric seismic monitoring is fraught with uncertainties. These DEMs typically contain errors and distortions on the order of the phenomena being investigated and furthermore must be precisely coregistered to the radar interferogram. Our approach in this paper is more readily quantifiable given the radar system parameters and can serve as a baseline for the design of a seismic monitoring program. Coregistration occurs automatically in forming the interferograms and the quality of the result can be measured "up front."

In addition to this fundamental difference in data manipulation, we extend and improve upon the previous results in other ways. In this study the entire usable phase field is "unwrapped," meaning that the displacement at each point is known digitally in an absolute sense, rendering the displacement field more amenable to computer modelling and analysis. This permits the precision of the technique to be increased from the 2.8 cm radar line of sight reported by Massonet to about 0.2 cm obtained here. Further, we verify the accuracy of the measurements by comparing to a displacement field derived from conventional surveying techniques. These survey data were derived from a combination of Electronic Distance Measurement (EDM) lines and Global Positioning

System (GI 'S) satellite receivers.

The structure of the paper is as follows. We begin by summarizing the theory of radar interferometry and differential interferometry, error sources, and (expectations of performance for seismic studies. Next we present the set of differential radar interferometric observations of the Landers earthquake, and discuss their accuracy. Finally, we compare our results with those of the earlier study and with the in situ measurements made by GPS techniques.

Summary of theory

Consider two radar systems observing the same ground swath from two positions A 1 and A2, respectively, as illustrated in figure 1. The measured phase at each point in each of the two radar images may be taken as equal to the sum of a propagation part proportional to the round-trip distance traveled and a scattering part due to the interaction of the wave with the ground. If each resolution element on the ground behaves the same for each observation (see more on this important condition below), calculating the difference in the phases removes dependence on the scattering mechanism and gives a quantity dependent only on geometry. If the two path lengths are taken to be ρ and $\rho + \delta\rho$, the measured phase ϕ will be

$$\phi = \frac{4\pi}{\lambda} \delta\rho \quad (1)$$

or 2π times the round-trip difference distance in wavelengths. The law of cosines permits solution for $\delta\rho$ in terms of the imaging geometry as follows. Then

$$(\rho + \delta\rho)^2 = \rho^2 + B^2 - 2\rho B \sin(\alpha - \theta) \quad (2)$$

where the baseline length is B , the range to a point on the ground is ρ , the look angle is θ , and the angle of the baseline with respect to horizontal is α . Neglecting the term of order $(\delta\rho)^2$ yields

$$\delta\rho \approx B \sin(\theta - \alpha) + \frac{B^2}{2\rho} \quad (3)$$

For simplicity in describing the approach we used, we can make a second approximation, although it is not necessary for the analyses presented below. In the case of spaceborne geometries we can ignore the second term on the right hand side of (3), and obtain

$$\delta\rho \approx B \sin(\theta - \alpha) \quad (4)$$

or

$$\delta\rho \approx B_{\parallel} \quad (5)$$

$B_{\parallel} = B \sin(\theta - \alpha)$ is simply the component of the baseline parallel to the look direction. This is the parallel-ray approximation used by Zebker and Goldstein (1986) in their initial paper on topographic mapping.

Equations (1) and (4) show that the measured phase of an interferometer is the component of the interferometer baseline parallel to the look direction to a given point, on the surface measured in wavelengths, multiplied by two for round-trip travel. We note that, the height sensitivity of the instrument enters through the dependence of the exact look angle θ on the altitude $z = h - \rho \cos \theta$, where h is the height of the sensor above the reference surface.

If a second (denoted prime) interferogram is acquired over the same area, sharing one orbit with the previous pair so that ρ and θ are unchanged (dashed lines in figure 1), we can compare the interferogram phases with each other. This second interferogram is acquired with a different baseline B' and baseline orientation α' , thus a different B_{\parallel}' . Combining (1) and (4) above we obtain

$$\phi' = \frac{4\pi}{\lambda} B_{\parallel}' \quad (6)$$

Examination of the ratio of the two phases yields

$$\frac{\phi}{\phi'} = \frac{B_{\parallel}}{B_{\parallel}'} \quad (7)$$

in other words the ratio of the phases is equal to the ratio of the parallel components of the baseline, independent of the topography

Now consider the situation of two interferograms acquired over the same region as before but in this case an earthquake has displaced each resolution element between observations for the primed interferogram. The displacements are assumed small with respect to a resolution cell so that the radar echoes remain correlated. Here in addition to the phase dependence on topography there is a phase change due to the radar line-of-sight component of the displacement $\Delta\rho$. In this interferogram the phase ϕ' will be given by

$$\phi' = \frac{4\pi}{\lambda} (B_{\parallel}' + \Delta\rho) \quad (8)$$

The displacement term $\Delta\rho$ adds to the topographic phase term, creating confusion in the interpretation of the result. However, if the data from the initial unprimed interferogram are properly scaled and subtracted from the primed interferogram, we can obtain a solution dependent only on the displacement of the surface, as follows

$$\phi' - \frac{B_{\parallel}}{B_{\parallel}'} \cdot \phi = \frac{4\pi}{\lambda} \Delta\rho \quad (9)$$

Since the quantity on the left is determined entirely by the phases of the interferograms and the orbit geometries, the line of sight component of the displacement $\Delta\rho$, is measurable for each point in the scene.

At this point we may consider the sensitivity of the phase measurement to the phenomena of topography and displacement, which may be derived by differentiating (8) with respect to height

through B_{\parallel} and displacement. In the first case, using $dz = \rho \sin \theta d\theta$, obtained from the dependence of height on angle described above, we find

$$d\phi' = \frac{4\pi}{\lambda} B \cos(\theta - \alpha) d\theta \quad (10)$$

and

$$\frac{d\phi'}{dz} = \frac{4\pi B \cos(\theta - \alpha)}{\lambda \rho \sin \theta} \quad (11)$$

For the displacement case we have

$$\frac{d\phi'}{d\Delta\rho} = \frac{4\pi}{\lambda} \quad (12)$$

Since the distance ρ typically is much greater than the baseline distance B , it is evident that equation (12) expresses a much more sensitive dependence of phase on height changes than (11). Comparing the two mu] ts numerically, for the April-August ERS-1 case described here (see next section) one meter of topography gives a phase signature of 4.3° , while for the same pass pair a one meter surface displacement yields a phase signature of 12800° , or nearly 3000" times greater sensitivity.

This ratio of sensitivities illustrates the power of the interferometric technique in detecting small changes. If, for example, we chose to map seismic displacements by differencing 1 DEMs, whether acquired interferometrically or by conventional stereo photogrammetry, changes would only be visible if they were significant in size compared to the uncertainty of the DEM measurement, which is typically meters. For the interferometric case in the previous paragraph, for example, system noise limits the useful signals to those causing a phase shift greater than about 20° , or 4.6 m. While thus permitting topographic mapping with a vertical precision of 4.6 m (see Zebker et al., 1993 for a discussion of ERS-1 DEMs with this precision), a worthwhile result for many applications, it is not particularly useful for the study of earthquakes. In contrast, if data are acquired with the interferometric pair spanning the seismic event, even 1 cm of line-of-sight displacement results in a signature of 64degrees, easily detectable in ERS-1 data.

There are, however, two very important limitations to the interferometric technique. First, radar echoes acquired on the three passes must correlate with each other, that is the signals must be substantially similar over a significant period of time. Physically this translates to a requirement that the ground scattering surface be relatively undisturbed at the radar wavelength scale between measurements. Several studies have addressed this phenomenon, both theoretically (for example, Li and Goldstein, 1990), and experimentally (for example, Gray et al., 1992). Zebker and Villasenor (1992) were able to model and quantify the temporal decorrelation process, and found that different surfaces decorrelate at different rates. This limits the applicability of the approach to areas that do not change much with time. Some regions, such as desert areas, may exhibit very little decorrelation over long periods. In the data presented here, correlation was usably high even after 105 days, the

longest time period examined. From this we conclude that the desert surface changes little over months if there is no appreciable weather.

The second limitation, more important for this study, is that the phases must be "unwrapped" before data from one interferogram may be used to correct the second interferogram (eq. 9 above) to estimate the displacement phases. The measurements of each phase are known only modulo 2π , and various techniques exist (Goldstein et al., 1988; E. Atsushi, personal communication, 1992, Ghiglia and Romero, 1993) to determine the absolute relationship between all the points in a scene (that is, unwrapping). While not fully characterized in any of the existing literature, it is apparent that the ability to unwrap arbitrary phase fields depends on two factors, the noise level in the system and the interferometric fringe spacing. For the July-August pair described here in particular, the interferometric baseline is quite large, 40 % of the critical baseline at which no correlation between signals is possible (for a more complete discussion on baseline decorrelation, see Zebker and Villasenor, 1992). Since the fringe rate depends on local surface slope, typically it is more difficult to estimate phases reliably in rough terrain than in flat terrain if the fringe rate is high to begin with. The result of this is that we were unable to obtain reliable phase estimates in the rougher regions, as will be seen in the data presented below.

ERS-1 Interferograms of the Landers Earthquake

We obtained raw ERS-1 radar signal samples acquired over the Landers region on April 24, July 3, and August 7, 1992. We combined these to form two interferograms, one from the April-August pair and one from the July-August pair. The April-August pair spans the June 28 earthquake, and was chosen over the April-July pair as the latter exhibited a baseline too large to work with. No data were acquired on May 29 when the satellite again passed over the site. Orbit reconstructions provided by the European Space Agency (ESA) enabled us to determine the geometrical parameters for the pairs chosen as follows:

Table 1. ERS-1 Orbit Parameters

| Pair | Baseline B | orientation α | Parallel component B_{\parallel} |
|--------------|------------|----------------------|------------------------------------|
| April-August | 146.1 | -117.9 | 96.0 |
| July-August | 503.1 | 265.6 | 454.3 |

The parallel components given in table 1 are for a look angle of 210° . Since the radar swath is quite wide, the actual look angle varies from about 17° to 23° and the parallel components vary somewhat.

A radar image of the Landers area is shown in figure 2, where the fault location is illustrated by the heavy line. These data, as well as the radar images below, are in a radar slant range and along track direction coordinate system. That is, the data have not been geocoded. We have preserved

the "natural" spacing of the data points in order to maintain the highest possible signal fidelity throughout the processing procedure. However, we do apply a geocoding transformation before comparison with the field survey results described in the following section.

We processed the raw signal samples at J1 'I, using a software processor constructed specifically for ERS-1 interferometric applications. The data were processed using a range-Doppler algorithm, but the range compressed signals were filtered for the July-August pair using the method suggested by Gatelli et al. (1993) to reduce baseline decorrelation. We found that this approach yielded about 5-10 % greater correlation in some regions at the expense of a slight reduction in range resolution.

The interferograms obtained in this process are shown in figure 3, with the corresponding correlation coefficient maps shown in figure 4. The upper image in each case represents the April-August interferogram, while the lower figure shows data from the July-August pair. The June 28 earthquake effects are found in the April-August pair. In these plots the fringe signature of a curved Earth surface has been removed from the interferograms for clearer display. Note that the very high fringe rates, and corresponding loss of correlation, in the mountainous regions for the July-August pair, lead to our inability to unwrap the phase in these regions. Also note in the April-August pair a similar loss of correlation in the fault zone, presumably due to i) very high fringe rates of greater than one cycle per resolution element, ii) large ground shifts resulting in lack of precision alignment of the pixels from pass to pass, and iii) stirring up of the surface at the wavelength scale from the earthquake itself.

These interferograms were filtered using a spatially variable bandpass filter that selected the optimal fringe rate passband in each 32 by 32 point subregion in the interferogram. In this process we also identified areas of low fringe visibility to serve as a mask in the final product, eliminating regions where we felt we could not trust the phase estimates. The data were then unwrapped using the method of Atsushi, which is an extension of the method first presented by Goldstein et al. (1988).

Finally, the differential interferogram was calculated by scaling the July-August measurement by the ratio of the parallel baseline components for each look angle and subtracting that value from the corresponding value in the April-August pair. The result is a map of the displacements of the ground in radar line of sight direction (equation 9), shown in figure 5, where the shift is coded by color and the brightness at each point is the radar image brightness. In addition, contour lines representing line of sight displacements spaced every 5 cm are shown.

It must be noted that the earthquake is not the only process affecting the phase measurements in this region of the Mojave. We show in figure 6 an enlargement of the April-August interferogram plus the correlation coefficients for a region east of Barstow where center-pivot irrigation has been employed. The irrigated circles, and some other agricultural fields, show a clear loss of correlation presumably due to crop growth, and phase shifts which are due to motion, not topography (it is a flat area). Gabriel et al. (1988) found similar surface displacements of several cm in fields that had

been irrigated over a nine day period. The motions observed in this image as well could be caused by changes in the surface elevations from pumping underground water or other hydrologic effects.

Since one of the strengths of this technique is its intrinsic high spatial resolution, we also show in figure 7 an enlargement in the April-August interferogram of a region around the fault zone. The phases in an interferogram are not unwrapped, and so should not exhibit discontinuities except in regions of severe layover unless discontinuous motions (breaks) occurred during the period spanned by the interferogram pair. Nevertheless, the figure shows clear discontinuities in relatively flat areas. For example, the region denoted A shows a clear break in the phase measurements. A similar break does not occur in the July-August pair and therefore it must be due to a displacement of the surface where one piece was displaced more than the other. This cracking effect is more pronounced in the region denoted B, shown enlarged again in figure 8, where the cracking is so extensive that it seems the ground has been broken into many tiles each several hundred meters across. These data are shown both in the wrapped, raw phase measurements at the left of the figure, and in unwrapped form on the right. In the case of the wrapped data, lines have been drawn in by hand to accentuate the boundaries of the tiles. The phase unwrapping algorithm we use must identify phase discontinuities before calculating the absolute phase values; the locations of cuts determined automatically by our algorithm are shown in black on the right hand side enlargement. Interestingly, the cuts are very much the same, but more extensive, than those drawn by hand. It would be an interesting field exercise to compare the computer generated cuts with any visible surface scars.

We also present in figure 9 a perspective view of the region where the vertical scale is proportional to the displacement in the radar line of sight of the surface. As usual, the brightness at each point is related to radar reflectivity, while the color is the displacement mapped into a repeating color table to accentuate the visibility of the changes to produce a contour-like map. From this view one can see that the displacement increases as the fault is approached at which point there is an abrupt break in the surface. Unfortunately the choice of perspective did not allow a good view of the region across the fault where the surface displacement was of opposite sign.

We assess the internal consistency and accuracy of the measurements presented here by three separate calculations. First, we calculate the expected errors due to statistical variation of the phase estimates. Assuming a signal to noise ratio of 6 dB for the flat desert surfaces, our 20 equivalent look processing yields a standard deviation of 9.50 for the geometry of the April-August interferogram and 14.50 for the July-August interferogram- these values follow from using a target radar cross section of -17 dB and accounting for losses accruing from illuminating the ground off the boresight of the antenna. Combining these yields an expected phase error of 100 rms for the differential interferogram, equivalent to a horizontal displacement noise due to finite signal to noise ratio and baseline decorrelation of 0.2 cm. We would expect this figure to be an underestimate as it does not take into account any temporal decorrelation due to surface disturbances or additional processing artifacts such as misregistration or other sampling and interpolation errors.

Second, we empirically determined statistical variations by measuring the observed phase standard deviations and converting the result to horizontal displacement errors. Choosing boxes in areas of little seismic variation yielded an average horizontal displacement of 0.4 cm rms for the high-frequency component of variations.

Finally, we attempted to address larger scale variations by measuring the displacement at ten widely separated locations far from the fault, and determined their standard deviation. This calculation gave a horizontal displacement error component of 0.6 cm rms for these medium frequency variations.

Comparison with field measurements

In this section we discuss the accuracy of our measurements and compare the results to those obtained in the field using Global Positioning Satellite (GPS) and Electronic Distance Measurement (EDM) survey data. It is not our purpose here to evaluate or analyze the accuracy of these field measurements. As a basis of comparison we will use the coseismic displacement field presented in the report of Freymueller et al. (1993), who derive the displacements from a combination of GPS data from several sources and EDM line lengths obtained by the USGS (please see the above reference for a more detailed description of the data sources and techniques). For simplicity we will refer to this combined data set and resulting derived displacement field as the GPS data set even though EDM data were also used to derive the displacement values.

The area of overlap between the field survey and our image contains 15 points at which both field data and radar estimates of the motion are available. Three additional site measurements of field data exist in the overlap region, but we were not able to obtain reliable radar phase estimates for them (they occur in the gray regions of figure 5). As can be seen from the figure, however, the radar data are generally valid over a wide area and should future surveys or analyses produce additional field points they may be easily compared with the present analysis.

As stated previously, the radar technique is sensitive to the line of sight component of motion. We therefore calculated the component of the GPS motion vectors in the direction of the projection of the radar sensor boresight on the Earth's surface. As for the radar measurements, since the line of sight direction is not in the plane defined by the local Earth surface, we derived the equivalent horizontal surface motion to yield the observed slant range displacement using

$$\Delta y = \frac{\Delta \rho}{\sin \theta} \quad (13)$$

which relates the horizontal displacement Δy to slant range displacement $\Delta \rho$ and the incidence angle θ . For this calculation we assumed the incidence angle is equal to 21° everywhere. The results of both of these calculations are shown in table 2 and figure 10 below.

Table 2. Comparison of Radar and GPS Motion Estimates

| Site | Component of GPS Vector in radar direction, cm | Horizontal displacement for observed radar motion, cm | Difference, cm |
|---------|---|--|----------------|
| OJD | 17.0 | 10.8 | 6.2 |
| FRY | 74.5 | 56.6 | 17.9 |
| ORD | 48.3 | 37.0 | 11.3 |
| DUMP | 20.4 | -5.0 | 25.4 |
| HARVARD | -0.3 | -1.0 | 0.7 |
| SOAP | 1.7 | 6.9 | -5.2 |
| FLASH | 12.0 | 8.6 | 3.4 |
| 6056 | 21.3 | 7.1 | 14.2 |
| MEANS | 68.3 | 108.7 | -40.4 |
| ROCK | 69.1 | 57.8 | 11.3 |
| 6052 | 33.2 | 41.1 | -7.9 |
| LUCS | 20.7 | 17.7 | 3.0 |
| POIN | 9.5 | 5.5 | 4.0 |
| STIM | 7.4 | 1.3 | 6.1 |
| 7000 | 91.1 | 18.6 | 72.5 |

The mean value of the differences in table 2 is 8.2 cm, and the rms difference is 23.8 cm. The formal correlation of the data is 0.70.

Figure 10 shows the same data of table 2 presented graphically. The area of overlap is shown by indicating the radar image edge as a set of crosses. For each survey site, denoted by a triangle, we illustrate vectors corresponding to motion as determined by survey techniques (diamond headed arrows) and as determined by the radar (cross headed arrows). Note that the radar vectors are all parallel to the edge of the radar image, as only the component of motion in the line of sight is measured.

From each of these presentations it is apparent that at most sites, with the significant exceptions sites 1 DUMP, 6056, and 7000, either the two values agree within 10 cm on an absolute scale or within $\approx 30\%$ on a relative scale. It is interesting to note that in each of the deviant cases a large motion is observed by the GPS technique, while a much smaller displacement is visible by the radar technique. In each case where a small motion is detected by the field survey, a small motion is measured by the radar interferometer. Figure 10 also suggests that there is a degree of spatial correlation in the regions of agreement, that is the amount of agreement is spatially dependent.

There are several possible causes for the disagreements in the measurements. First, the radar technique is highly sensitive to vertical motions which are not expressed in the GPS displacement

field. While this is likely to affect the differences on the cm scale, it is probably not a significant factor in the radar underestimation of the motions. This follows from the unlikelihood that vertical motions would just happen to be in the direction with respect to the radar to cancel out any horizontal shifts.

The second cause for disagreement is error in the measurements. As discussed above, the radar data exhibit statistical errors less than 1 cm rms on both small and medium scales, thus would be insignificant for this comparison. However, large scale warping of the radar image remains a possibility. We were able to remove most of these effects by examining the parts of the image far from the earthquake at the left and top of figure 5 and removing obvious biases. If the ERS-1 coverage had been such that the fault was positioned in the center of the radar swath, we could have applied a similar correction more accurately all the way around the image. The possibility of a long scale error thus still exists, and may to some degree explain the observed spatial correlation of the errors.

We are unable to assess the expected errors in the GPS data set in detail, however discussion with the GPS team (P. Segall, personal communication) indicates that these errors should not exceed one or two cm.

A third possibility is the existence of phase unwrapping errors in the radar data. As each unwrap error results in a one cycle phase error in one interferogram, these errors would appear as $\frac{\lambda}{2}$ errors in $\Delta\rho$, or 8 cm in horizontal shift if it occurred in the April-August pair or 2 cm in the July-August pair. However, we have examined the data for signs of unwrapping errors and believe that the regions near the GPS sites are unwrapped correctly. In addition, it is unlikely again that phase unwrapping mistakes would nearly correct for GPS-observed displacements.

Finally, the locations of the GPS sites are known only approximately in the radar image as the radar data are not geocoded, thus leading to estimates at the wrong places. However, we have analyzed the regions around the sites in the radar data and have determined that the displacement does not change rapidly in those areas. Thus, even a slight positional shift would not result in a significant error.

Discussion

We have shown that it is possible to map a coseismic displacement field resulting from a major earthquake using only data acquired from an orbiting high resolution radar system, and achieve results similar in accuracy to those obtained by conventional field survey techniques. Data from the ERS-1 synthetic aperture radar instrument acquired at three separate instances of time are sufficient to generate a high resolution, wide area map of the displacements. Comparison of these data with GPS and EDM survey data indicate a high degree of confidence in the radar measurements. We are confident that the differences between the radar and GPS measurements are reconcilable and do not point to a fundamental limitation in the radar technique. Further work is needed along

these lines however.

The power of the differential interferometry technique for seismological applications lies in its cm-scale measurement sensitivity of line-of-sight displacements over a wide area. The derived displacement fields can be used as a tight constraint in the modeling of earthquake motion. The fine accuracy, fine spatial resolution, and large areal coverage will likely allow increasingly detailed models to be explored, on both large and small spatial scales. The promise of a system to map small scale fractures in the Earth's surface over a wide region automatically with a remote sensing system will greatly facilitate field activities by permitting concentration in the most important areas.

In addition to after the fact seismic event modeling, there is promise that radar interferometry can become a predictive tool. For example, volcanoes are known to bulge prior to eruption. If similar small scale displacements precede seismic events, it may be possible to bracket the time of occurrence more precisely than by conventional methods. No evidence to our knowledge exists that motion precedes seismic events, however the sparseness and limited accuracy of detection survey methods may not allow a definitive conclusion. Several groups are pursuing this line of research, by studying, interferometric displacement data in several areas of likely seismic activity,

One can envision a global seismic satellite mission designed to predict and detect earthquakes: a single satellite in a short repeat period orbit similar in design to that proposed by Zebker et al, (1993) for global topographic mapping. The repeat cycle of the orbit should be short, on the order of 1 day, to minimize the effects of temporal decorrelation. Precise satellite ephemeris from GPS measurements can ensure automatic construction of interferograms and displacement fields. Only thin repeat periods of data need to be stored at any time; the processing can proceed in real time and results can be processed automatically for evidence of anomalous displacements. Detailed design of the radar system, orbital scenario, the establishment of detection and false alarm thresholds must await interest by the global community. Given the enormous cost in lives and resources inflicted by earthquakes, interest is sure to follow any evidence that radar interferometry can be used predictively.

Acknowledgements

We would like to acknowledge Paul Segall for supplying the GPS/EDM measurements and for several useful discussions regarding the intercomparison of the data sets. The research described in this paper was carried out, by the Jet Propulsion Laboratory, California Institute of Technology, under a contract with the National Aeronautics and Space Administration.

REFERENCES

- Evans, J. L., T. G. Farr, H. A. Zebker, and J. M. Mougini-Mark, Radar interferometric studies of the Earth's topography, *EOS*, Vol. 73, No. 52, pp. 553 and 557-558, December 29, 1992.
- Freymueller, J., N. E. King, and P. Segall, The coseismic slip distribution of the Landers earthquake, submitted to *Bull. Seism. Soc. Am.*, 1993.
- Gabriel, A. G., R. M. Goldstein, and H. A. Zebker, Mapping small elevation changes over large areas: I Differential radar interferometry, *J. Geophys. Res.* 94, No. 117, 9183-91, July 10, 1989.
- Gatelli, F., A. Monti Guarnieri, F. Parizzi, P. Pasquali, C. Prati, and F. Rocca, Use of the spectral shift, in SAR interferometry: applications to ERS-1, submitted to *IEEE Transactions on Geoscience and Remote Sensing*, 1993.
- Ghiglia, D. C., and J. Romero, Robust two-dimensional weighted and unweighted phase unwrapping using fast transforms and iterative methods, in press, *J. Opt. Soc. Am.*, 1993.
- Goldstein, R. M., and H. A. Zebker, Interferometric radar measurement of ocean surface currents, *Nature* 328, 707-9, August 20, 1987.
- Goldstein, R. M., H. A. Zebker, and C. L. Werner, Satellite radar interferometry: two dimensional phase unwrapping, *Radio Science* 23, No. 4, 713-720, July-August 1988.
- Goldstein, R. M., P. Barnett, and H. A. Zebker, Remote sensing of ocean currents, *SCIENCE*, Vol 246, 1282-85, December 8, 1989.
- Gray, A. Laurence and P. J. Farris-Manning, Two-pass interferometry with airborne synthetic aperture radar, submitted to *IEEE Trans. Geo. Rem. Sens.*, 1991.
- Li, P. and R. M. Goldstein, Studies of multi-baseline spaceborne interferometric synthetic aperture radars, *IEEE Trans. Geo. Rem. Sens.*, vol. 28, no. 1, pp. 88-97, January 1990.
- Madsen, S. N., H. A. Zebker, and J. Martin, Topographic mapping using radar interferometry: processing techniques, *IEEE Trans. Geosci. Rem. Sensing*, Vol. 31, no. 1, January, 1993a.
- Madsen, S. N., J. Martin, and H. A. Zebker, Analysis and evaluation of the NASA/JPL TOI SA 1 R across-track interferometric SAR system, submitted to *IEEE Transactions on Geoscience and Remote Sensing*, October, 1993b.
- Massonnet, D., M. Rossi, C. Carmona, F. Adragna, G. Peltzer, K. Feigl, and P. Rabaute, The displacement field of the Landers earthquake mapped by radar interferometry, *Nature* 364, No. 6433, pp. 138-142, 1993.

- Prati, C., F. Rocca, A. Monti Guarnieri, and E. Damonti, Seismic migration for SAR focusing: interferometrical applications, *IEEE Transactions on Geoscience and Remote Sensing*, Vol 28, no 4, July 1990.
- Zebker, H. A., and R. M. Goldstein, Topographic Mapping Derived from Synthetic Aperture Radar Measurements, *J. Geophys. Res.* 91, 4993-9, 1986.
- Zebker, H. A., and J. Villasenor, Decorrelation in interferometric radar echoes, *IEEE Trans. Geo. Rem. Sensing*, Vol 30, no. 5, pp 950-959, September, 1992.
- Zebker, H. A., S.N. Madsen, J. Martin, K.B. Wheeler, J. Miller, Y. Lou, G. Alberti, S. Vetro, A. Cucci, The TOPSAR interferometric radar topographic mapping instrument, *IEEE Transactions on Geoscience and Remote Sensing*, Vol 30, no. 5, pp 933-940, September, 1992.
- Zebker, H. A., C.J. Werner, P. Rosen, and S. Hensley, Accuracy of topographic maps derived from ERS-1 radar interferometry, submitted to *IEEE Transactions on Geoscience and Remote Sensing*, April, 1993.

Figure captions.

Figure 1. Radar imaging geometry. The solid lines show that radar signal paths for the first interferogram pair formed by antennas at A1 and A2. Dashed lines show signal path for second interferogram acquired over the same site but with antennas located at A1' and A2'.

Figure 2. Radar image of the Landers area, where the fault location is illustrated by the heavy line and cities of Barstow, Victorville, and the Lucerne Valley area are shown for reference. These data, as well as the radar images in the remaining figure, are in a radar slant range and along track direction coordinate system.

Figure 3. Interferograms of the Landers area. The upper image is the April-August interferogram, while the lower image shows data from the July-August pair. The June 28 earthquake effects are found in the April-August pair. The fringe signature of a curved Earth surface has been removed from the interferograms for clearer display. Note the very high fringe rates in the mountainous regions for the July-August pair, leading to our inability to unwrap the phase in these regions.

Figure 4. Corresponding correlation coefficient maps to interferograms of figure 3. Note in the April-August pair a loss of correlation in the fault zone, presumably due to i) very high fringe rates of greater than one cycle per resolution element, ii) large ground shifts resulting in lack of precision alignment of the pixels from pass to pass, and iii) stirring up of the surface at the wavelength scale from the earthquake itself.

Figure 5. Differential interferogram of the Landers earthquake region. Radar line of sight

displacements are coded in color, ranging from -71 to 70 cm, while the radar reflectivity of the surface is shown as brightness. Contours indicating each 5 cm of displacement are drawn in black.

Figure 6. Enlargement of the April-August interferogram plus the correlation coefficients for a region east of Barstow where center-pivot irrigation has been employed. The top image is radar reflectivity, the center is correlation coefficient, and the lower image is the unwrapped interferogram. Black spots in the lower image are where correlation was insufficient for reliable phase estimates. The irrigated circles show a clear loss of correlation, presumably due to crop growth, and phase shifts which are due to motion, not topography. Examination of the mountains at the top left of the image shows that a topographic change of over 150 m is necessary to cause a one cycle change in phase, and the area in question shows less than 30 m variation. These phase changes could be caused by changes in the surface elevations from pumping underground water or other hydrologic effects.

Figure 7. Enlargement in the April-August interferogram of a region around the fault zone. The region denoted A shows a clear break in the phase measurements, which must be due to a displacement of the surface where one piece was displaced more than the other. More extensive cracking is found in region B (see next figure).

Figure 8. Region B from previous figure. Cracking is so extensive that it seems the ground has been broken into many tiles each several hundred meters across. At left, unwrapped, raw phase measurements, and at right, data in unwrapped form. In the case of the wrapped data, lines have been drawn in by hand to accentuate the boundaries of the tiles. The phase unwrapping algorithm we use also must identify phase discontinuities before calculating the absolute phase values, and the locations of cuts determined automatically by our algorithm are shown in black on the right hand side enlargement. The tiles are very much the same, but more extensive, than those plotted by hand.

Figure 9. Perspective view of the region where the vertical scale is proportional to the surface displacement in the radar line of sight. The brightness at each point is related to radar reflectivity, while the color is the displacement mapped into a repeating color table, producing a contour-like map. The color repeat interval is approximately 10 cm. The displacement increases as the fault is approached at which point there is an abrupt break in the surface,

Figure 10. Displacement vectors as measured by GIS / EDM data and by radar interferometry. Vectors are correlated at 0.74 level, and show that radar and field surveys are measuring similar phenomena.



figure 2 zebker and rosen



Figure 3
Zehker and Rosen

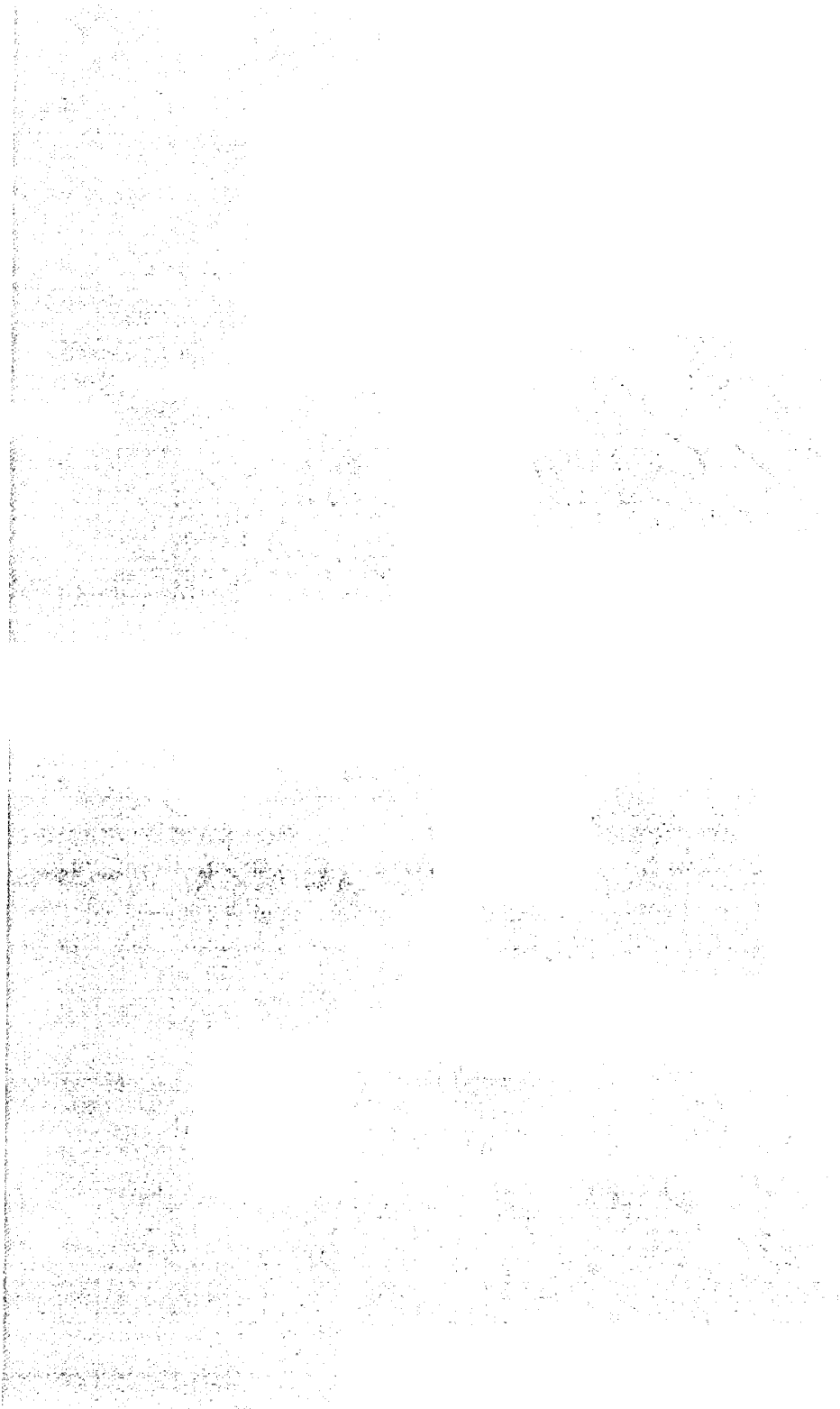


Figure 4
Zebker and Rosen

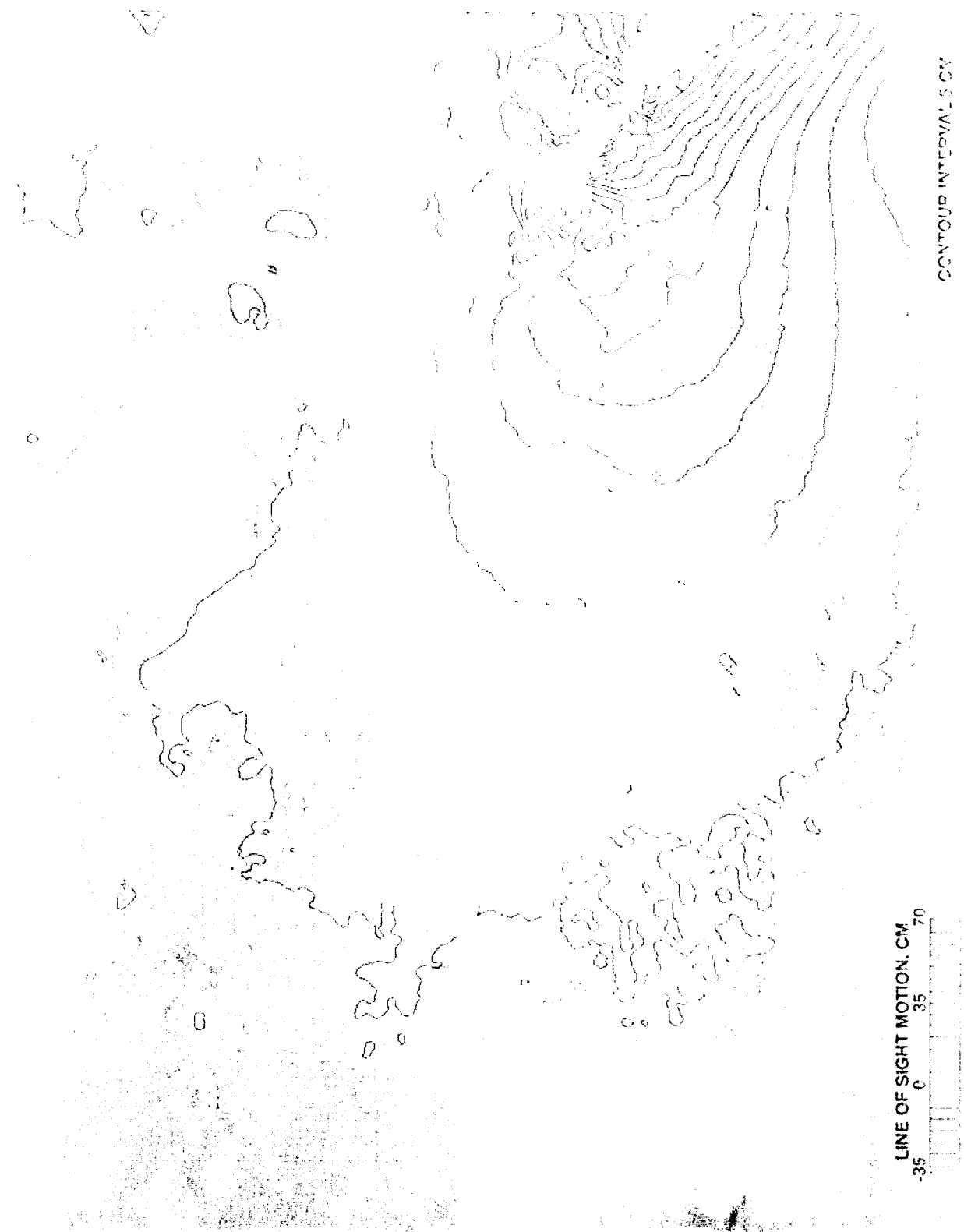


Figure 5
Zebker and Rosen



Figure 6
Zebker and Jensen

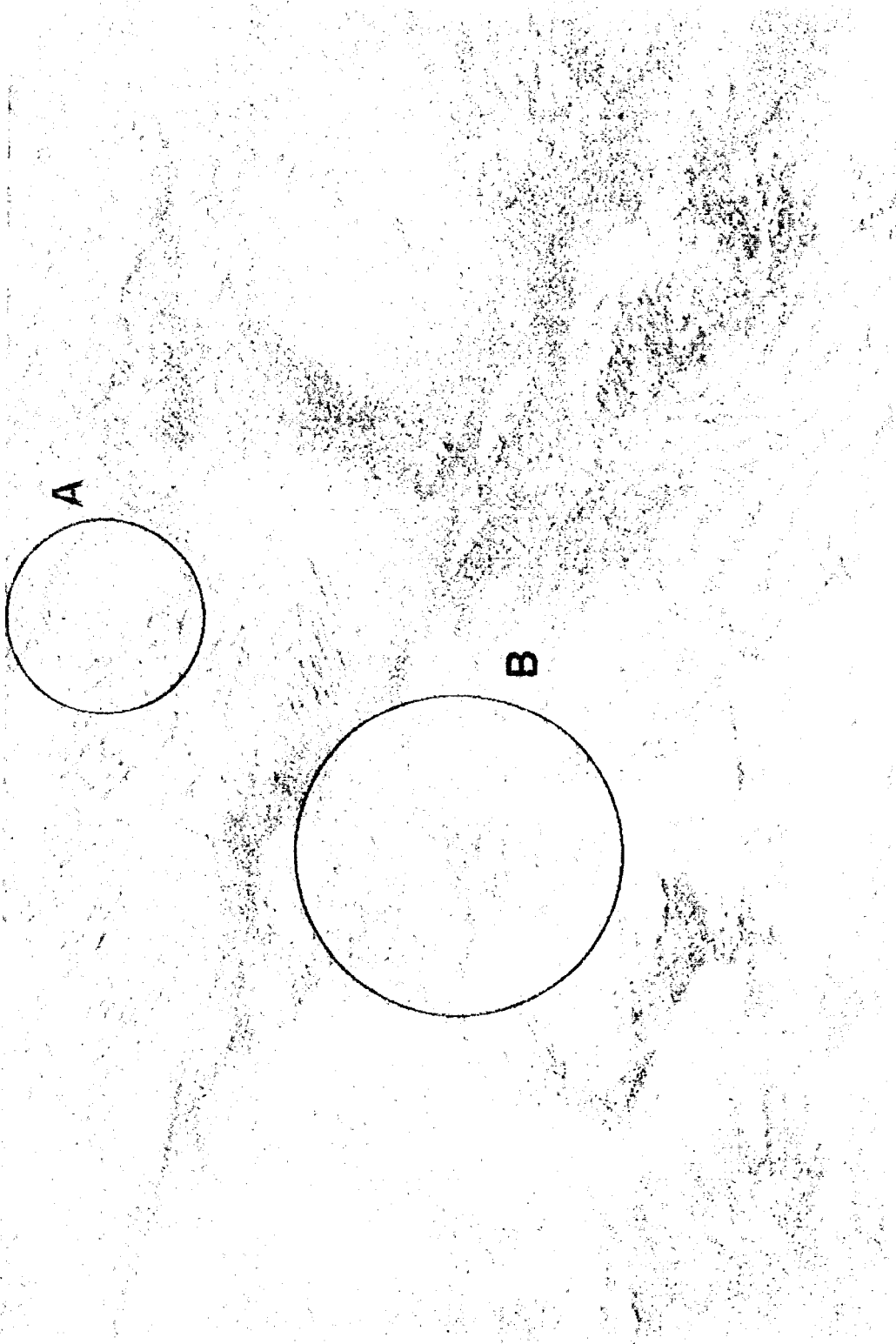


Figure 7
Zebker and Rosen

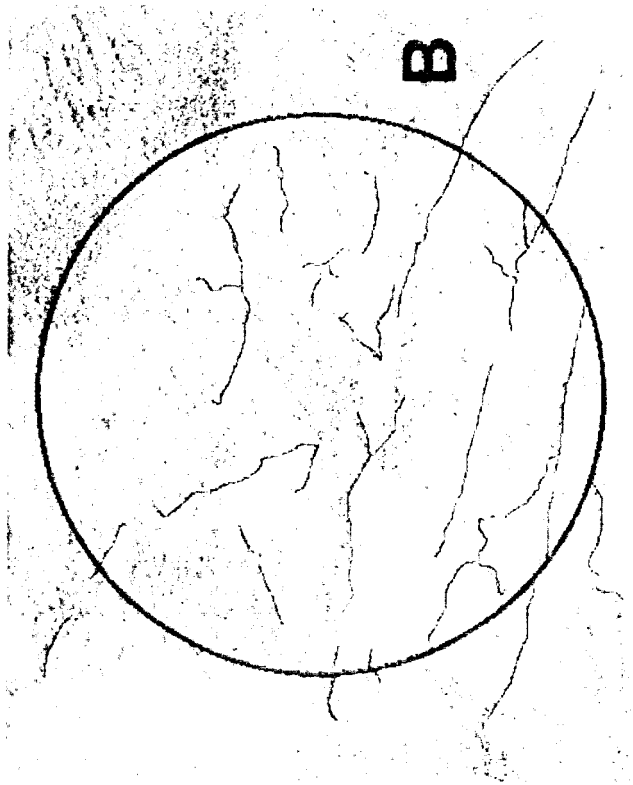
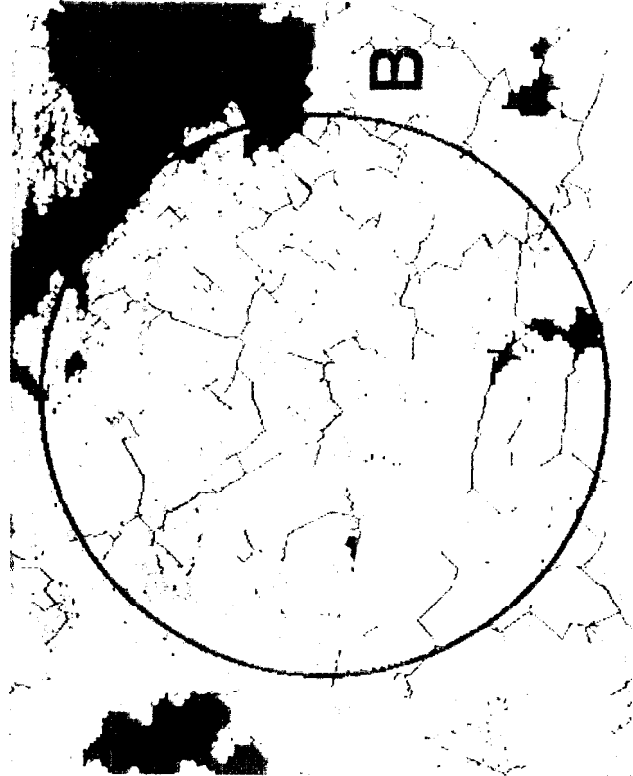


Figure 8
Zebker and Rosen

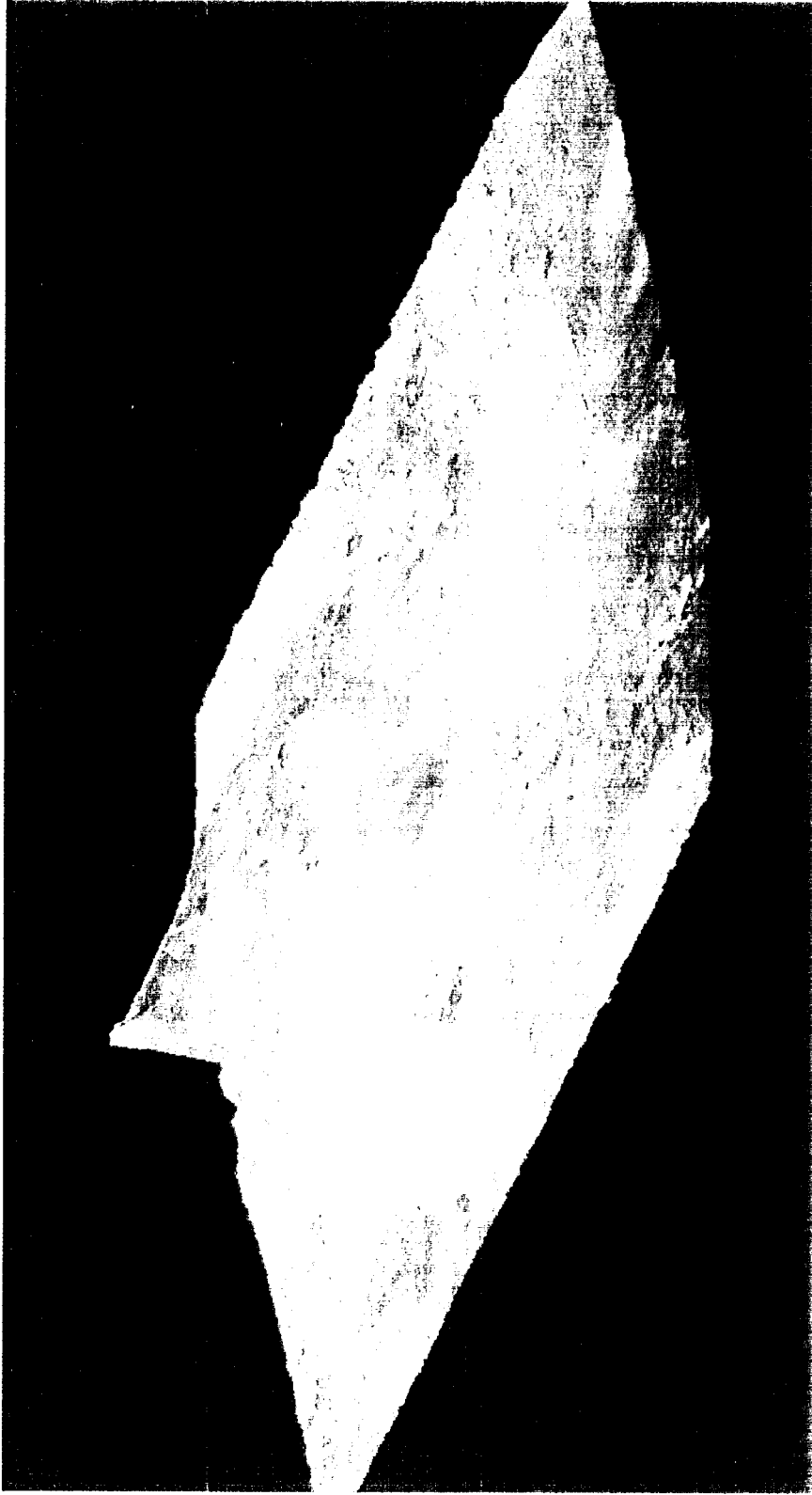


Figure 9
Zebker and Rosen

GPS AND RADAR DISPLACEMENT VECTORS

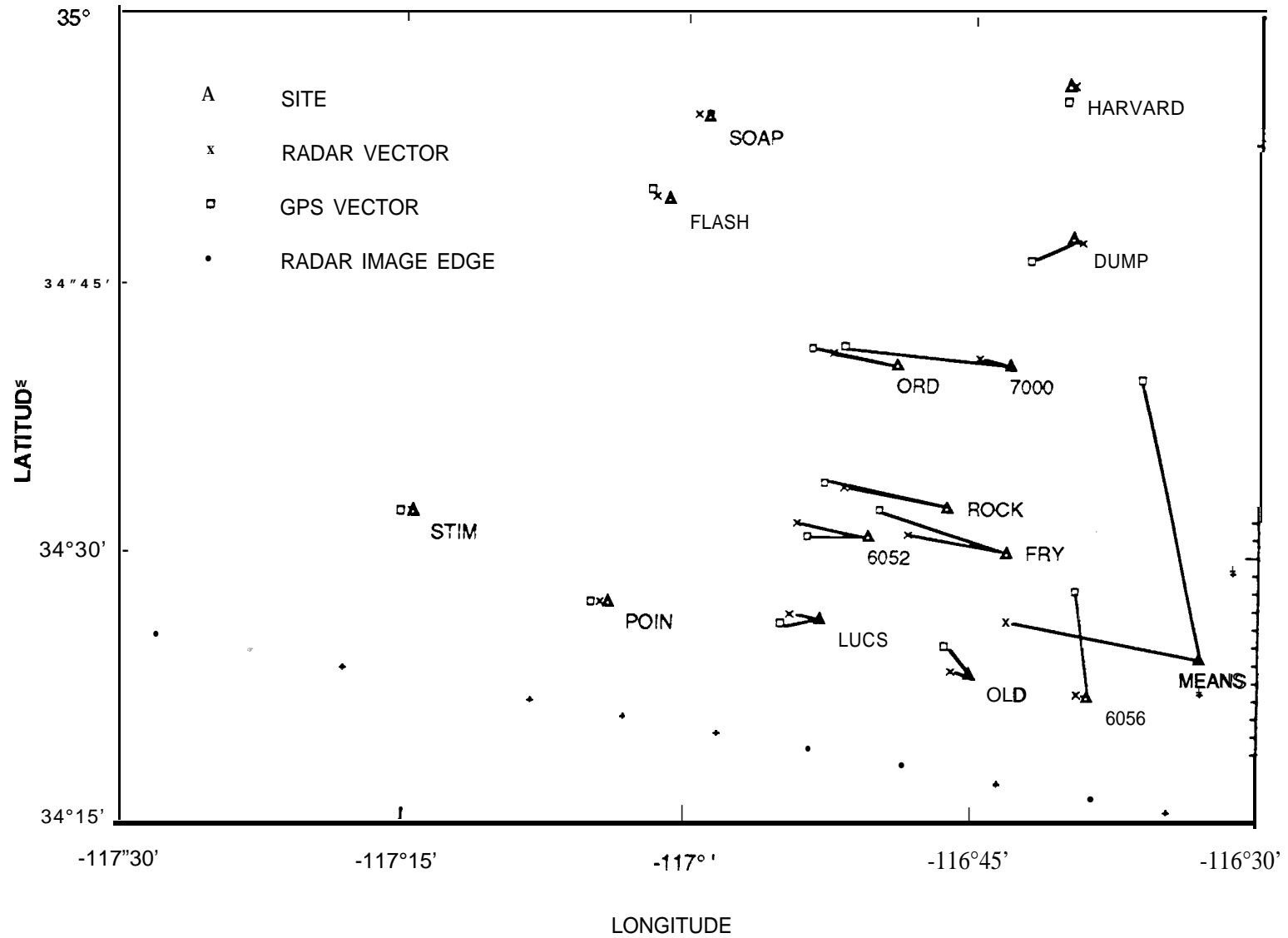


Figure 10. Zebker and Rosen, 1993